

# Information Sifting Funnel: Privacy-preserving Collaborative Inference Against Model Inversion Attacks

Rongke Liu\*

Nanjing University of Aeronautics and Astronautics  
Nanjing, China  
liurongke@nuaa.edu.cn

## ABSTRACT

The complexity of neural networks and inference tasks, combined with the demand for computational efficiency and real-time feedback, poses significant challenges for resource-constrained edge devices. Collaborative inference addresses this by delegating shallow feature extraction to edge devices and uploading feature to the cloud for subsequent inference tasks, reducing computational pressure. However, the transmitted features remain vulnerable to model inversion attacks (MIAs), which can reconstruct original input data. Existing defenses, including perturbation and information bottleneck techniques, provide explainable protection but are limited by the lack of standardized criteria for evaluating MIA difficulty, challenges in mutual information estimation, and trade-offs among usability, privacy, and deployability.

To overcome these limitations, we establish the first criterion for assessing the difficulty of MIAs in collaborative inference, supported by theoretical analysis of existing attacks and defenses and validated through experiments using the Mutual Information Neural Estimator (MINE). Building on these findings, we propose SiftFunnel, a privacy-preserving framework for collaborative inference. Specifically, we first train the edge model with both linear and non-linear correlation constraints to limit redundant information in transmitted features, enhancing privacy protection. Moreover, label smoothing and a cloud-based upsampling module are incorporated to balance usability and privacy. To further support deployability, the edge model is designed with a funnel-shaped structure and integrates attention mechanisms, preserving both privacy and usability. Extensive experiments show that SiftFunnel outperforms state-of-the-art defenses against MIAs, achieving superior privacy protection with less than 3% accuracy loss and an optimal trade-off among usability, privacy, and practicality.

## CCS CONCEPTS

• Security and privacy → Domain-specific security and privacy architectures.

## KEYWORDS

Collaborative inference, model inversion attacks, deep learning security and privacy, information theory

### ACM Reference Format:

Rongke Liu. 2025. Information Sifting Funnel: Privacy-preserving Collaborative Inference Against Model Inversion Attacks. In *Proceedings of ACM Conference on Computer and Communications Security (CCS'25)*. ACM, New York, NY, USA, 15 pages. <https://doi.org/XXXXXXXX.XXXXXXX>

## 1 INTRODUCTION

The rapid advancement of deep learning has led to increasingly complex and powerful neural network models, enabling remarkable performance in tasks such as image detection and recognition, speech processing, and natural language understanding. However, these advancements also pose significant challenges for edge computing devices [24]. In fields such as intelligent transportation, autonomous driving, facial recognition, IoT applications involving cameras and sensors, and remote healthcare monitoring, edge devices must process data instantly while handling growing computational demands. The limited resources of edge devices make it difficult for them to efficiently perform complex deep learning inference tasks independently [39].

Cloud computing enables inference by uploading data to cloud-based models, offering significant computational power. However, it faces two key limitations: bandwidth and network latency hinder its ability to meet real-time application requirements, and uploading raw data raises privacy concerns, especially in sensitive scenarios. Collaborative inference (CI) [40] has emerged as a viable solution to these challenges. By partitioning a neural network into  $f_{\text{edge}}$  and  $f_{\text{cloud}}$ , the edge device processes raw inputs into feature representations via  $f_{\text{edge}}$ , which are then uploaded to the cloud for further inference by  $f_{\text{cloud}}$ . This approach balances real-time performance and computational efficiency. In recent years, this technique has garnered attention in practical applications, such as unmanned aerial vehicles (UAVs) [35] and IoT systems [39], as well as in solutions like Apple's private cloud computing (PCC) [11]. With advancements in 5G, IoT, and AI, collaborative inference holds promise for broader adoption and future impact.

However, recent studies have revealed significant privacy risks in collaborative inference, where input data on edge devices can be reconstructed through model inversion attacks (MIAs) [19, 50, 52], as shown in Figure 1. MIAs are fine-grained privacy attacks that leverage the output information of AI models and deep learning generation techniques to reconstruct input data [19, 51], recover representative training data [28, 56], or expose sensitive information [13, 30]. These risks are particularly severe in collaborative inference scenarios. The root cause is that, compared to centralized

Permission to make digital or hard copies of all or part of this work for personal or classroom use is granted without fee provided that copies are not made or distributed for profit or commercial advantage and that copies bear this notice and the full citation on the first page. Copyrights for components of this work owned by others than the author(s) must be honored. Abstracting with credit is permitted. To copy otherwise, or republish, to post on servers or to redistribute to lists, requires prior specific permission and/or a fee. Request permissions from [permissions@acm.org](mailto:permissions@acm.org).  
CCS'25, October 13–17, 2025, xx, xx

© 2025 Copyright held by the owner/author(s). Publication rights licensed to ACM.  
ACM ISBN 978-1-4503-XXXX-X/25/10...\$15.00  
<https://doi.org/XXXXXXXX.XXXXXXX>

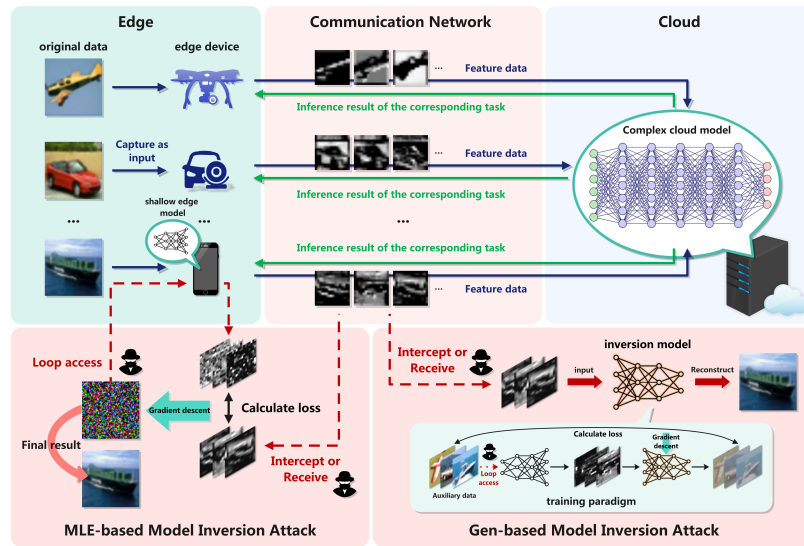


Figure 1: Collaborative inference and the threat of model inversion attacks.

model deployment, edge devices typically employ shallow neural networks to compute and upload feature representations. These features contain far more information than the final inference results, enabling adversaries to reconstruct the input data [3]. For instance, in facial recognition applications, while adversaries in centralized deployments might only recover training data through the model’s API [42, 53], those in collaborative inference can directly reconstruct the raw facial data collected by edge devices from the transmitted features.

The model inversion attack in collaborative inference can be divided into two types based on their technical approaches: Maximum Likelihood Estimation (MLE-based) MIA [19, 20] and Generative Deep Learning Model-based (Gen-based) MIA [20, 52]. MLE-based MIA minimizes the loss between the edge model’s output and the transmitted features by iteratively optimizing the input to closely match the transmitted features, thereby reconstructing original input data that are nearly indistinguishable from the real data. This approach performs effectively on shallow neural networks and low-complexity linear models but relies on the assumption of white-box access to the edge model for gradient-based optimization, which limits its applicability in practical scenarios. To address these limitations, Gen-based MIA employs a generator to approximate the inverse mapping function of the edge model, achieving  $\text{Data} \approx \text{Generator}(\text{Feature})$ . This method is effective when the generator’s training data distribution approximates the input data distribution of the edge model and the generator has sufficient capacity to model the inverse function. The privacy risks posed by MIA have prompted significant research into defense mechanisms, yet challenges remain in analyzing theoretical attacks and balancing usability, privacy preservation, and deployment feasibility.

Firstly, existing defense techniques in collaborative inference lack a thorough and unified analysis of the fundamental nature of MIA. Current mainstream defense methods can be categorized into three types based on their technical approaches: perturbation-based [20, 46], information bottleneck (IB)-based [34, 47], and neural

network depth & information bottleneck (NND & IB)-based defense strategies [3, 8]. Perturbation-based strategies aim to increase the difficulty of attacks by introducing perturbations to the gradients or output information of the trained model. IB-based strategies focus on approximating the reduction of mutual information  $I(x, z)$  between the input data  $x$  and the feature  $z$ , thus minimizing redundant information about  $x$  in  $z$  [45]. NND & IB-based strategies leverage the observation that increasing the depth of the edge network can induce an information bottleneck effect, thus enhancing defense. These methods provide theoretically interpretable defense mechanisms, with the introduction of information theory concepts offering notable contributions to defense design. However, existing work lacks a comprehensive understanding of MIA, relies on weak assumptions about adversarial capabilities, and fails to establish a clear criterion for evaluating the complexity of implementing MIA. As a result, defenses against MIAs still have room for improvement, including addressing potential future advancements.

Secondly, the trade-off between usability, privacy, and deployability in edge models remains a challenging and underexplored area in current research. Encryption-based defense strategies receive limited attention in collaborative inference due to resource constraints and the need for multitask processing in real time [31]. Additionally, encryption does not guarantee complete data security, as modern side-channel attacks leveraging deep learning can recover encrypted data [22]. The three main defense strategies discussed above also face issues of imbalance. Perturbation-based methods often compromise usability, whereas IB-based defenses aim to reduce mutual information  $I(x, z)$ , providing theoretical protection against simpler attacks such as MLE-based MIA. However, accurately computing  $I(x, z)$  is challenging, as it relies on approximations through sufficient data and specific algorithms, making it less effective against more advanced attacks such as Gen-based MIA. Adversarial training has been introduced as a component to address the aforementioned issues, but its strong specificity and limited interpretability make it difficult to prevent future advanced

attacks while significantly increasing the difficulty of training edge models. The NND & IB-based approach aims to balance privacy and usability by increasing model depth, but this approach significantly raises the resource demands on edge devices, including memory, storage, and bandwidth, thereby reducing deployability. As a result, such methods are often less favored in practical applications.

Thus, there is a pressing need for a novel approach grounded in an in-depth analysis of attack theories to provide interpretable and effective privacy protection while maintaining the usability and deployability of edge models. This need gives rise to three key technical challenges. *Challenge 1: How to establish an experimentally validated criterion for assessing MIA difficulty in collaborative inference?* Prior studies have interpreted MIA from an information-theoretic perspective, but challenges in computing mutual information and conducting an in-depth analysis of attack principles have hindered the establishment of a verifiable criterion, which is essential for guiding defense design and evaluating methods. *Challenge 2: How to effectively and interpretably remove redundant information from transmitted features while preserving edge model usability?* Although information bottleneck theory provides an interpretable defensive effect, mutual information is challenging to calculate, and current approximation methods are suboptimal. *Challenge 3: How to balance usability and privacy while ensuring practical deployability?* NND & IB-based methods significantly increase computational overhead on edge devices, making them challenging for practical application. Moreover, when applied to edge models that perform only simple feature extraction, these methods also struggle to resist advanced Gen-based MIAs.

To overcome the aforementioned challenges, we established a criterion  $D_{mia}$  for evaluating the difficulty of MIAs in CI and proposed a lightweight privacy-preserving strategy called Information Sifting Funnel (SiftFunnel), incorporating three key features. (1) *SiftFunnel provides interpretable defense principles based on  $D_{mia}$ .* We identified factors influencing attack difficulty in collaborative inference, including  $I(x, z)$  and the effective information mean  $\delta(z)$ , i.e., the average number of non-zero elements in  $z$ . By analyzing these factors, we clarified defense design directions and developed a framework to address potential future threats. Using the Mutual Information Neural Estimator (MINE) [4], we quantified the changes in  $I(x, z)$  at different network depths, validating the criterion. (2) *SiftFunnel effectively reduces redundant information in transmitted features while preserving edge model usability.* Guided by the proposed criterion, we enhanced the model’s loss function to include distance-correlation and Pearson-correlation measures, alongside an  $l_1$ -norm constraint on  $z$ . These refinements reduce  $H(z)$ ,  $\delta(z)$  while increasing  $H(x|z)$ . To further filter redundant information, we integrated Squeeze-and-Excitation (SE) Modules [23], Triple Attention Mechanisms [32], and Convolutional Block Attention Modules (CBAM) [48] into the edge model to focus on task-relevant features. Usability was preserved through a combination of label-smoothing and KL-divergence loss. (3) *SiftFunnel balances usability and privacy while light-weighting the edge model.* A funnel-shaped edge model was designed to progressively reduce transmitted channels, improving efficiency and reducing redundant information while minimizing memory and storage demands. To maintain usability, an upsampling module was added on the cloud side.

Based on prior evaluation metrics, this paper incorporates  $I(x, z)$ , quantified using MINE, and  $\delta(z)$  as key metrics to validate the theoretical analysis and assess the effectiveness of defense methods. To evaluate deployability, we consider the edge model’s parameter count, memory usage, storage consumption, and inference latency. Through extensive experiments, we demonstrate the validity of the proposed difficulty criterion and the effectiveness of SiftFunnel in balancing usability, deployability, and data privacy compared to existing methods.

Our contributions are summarized as follows.

- We establish the first difficulty criterion for implementing MIA in collaborative inference, providing guidance for defense design and preventing future advanced MIAs.
- We propose SiftFunnel, a privacy-preserving scheme for collaborative inference that constrains redundant transmitted features through linear and nonlinear correlation, ensuring model usability with label smoothing and loss function regularization.
- SiftFunnel adopts a funnel-shaped structure with integrated attention mechanisms to balance usability and privacy while maintaining the deployability of edge models.
- We conduct systematic experiments validating the proposed criterion and demonstrating SiftFunnel’s advantages in balancing usability, privacy, and deployability.

## 2 BACKGROUND AND RELATED WORK

### 2.1 Collaborative inference

The rapid development of artificial intelligence has enabled deep learning models to achieve exceptional performance in image processing and other tasks. However, the computational demands of these models often exceed the capabilities of resource-constrained edge devices, which face limitations in processing power, storage, and energy efficiency. To address these challenges, collaborative inference [40] has emerged as an effective solution. This approach divides the inference process into two stages: one part is performed locally on the edge device (which may consist of a single device or a chain of interconnected devices), while the remaining computation is uploaded to the cloud. Formally, this can be expressed as

$$f(x) = f_e(x) \circ f_c(f_e(x)) \quad (1)$$

where  $f$  is the full trained model,  $x$  is the input,  $f_e$  represents the model deployed on the edge, and  $f_c$  corresponds to the portion deployed in the cloud.

Collaborative inference typically begins with training  $f$  on centralized datasets in the cloud, followed by partitioning and deploying the  $f_e$  to the edge. Alternatively, methodologies such as Split Learning [58] enable edge devices to participate in model training locally. Regardless of the training approach, the inference process remains consistent. As depicted in Figure 1, the edge-deployed model first computes an intermediate representation  $feature = f_e(x)$ , which is then transmitted to the cloud for completion of the inference process  $result = f_c(feature)$ . The final output is either sent back to the edge device or retained in the cloud for further analysis.

Compared to the traditional approach of uploading raw data to the cloud for inference, collaborative inference offers distinct

advantages. First, it reduces communication overhead by allowing the transmitted features to be processed, potentially making them smaller in size than the original data. Second, it improves privacy protection by limiting the exposure of sensitive information by transmitting processed features instead of raw data, such as physiological signals or facial images. These advantages make collaborative inference a suitable solution for applications in health-care, facial recognition, and industrial IoT, where efficiency and privacy are critical requirements.

However, existing research highlights that collaborative inference models are susceptible to Model Inversion Attacks (MIA), where adversaries attempt to reconstruct the original input data from transmitted feature. Notably, in edge-based inference, computations can be distributed across multiple devices in a chained architecture [19], expressed as  $f = f_{e1} \circ f_{e2} \dots \circ f_c$ . Studies show that deeper neural networks exhibit greater resistance to data reconstruction, making devices positioned closer to the cloud less vulnerable. In contrast, the initial edge device, which typically employs a shallow neural network for feature computation and transmission, generates representations that retain more information from the original input, increasing its susceptibility to MIA. Given this vulnerability, this paper focuses on the MIA threat to the initial edge device, which uses a shallow neural network while the rest resides in the cloud. This common scenario in real-world applications poses a significant security risk due to the heightened likelihood of input data reconstruction, underscoring the need to address this challenge.

## 2.2 Model inversion attack

Model Inversion Attack (MIA) is a fine-grained privacy attack that uses the output of a target model and adversarial knowledge, such as white-box access or training data distribution, to reconstruct training data [56], sensitive attributes [30], or input data [51]. Initially proposed by Fredrikson et al. [12], MIA was applied to linear regression models, successfully reconstructing genomic data from warfarin dosage predictions and patient attributes, thereby revealing the privacy risks. Subsequent studies [12] extended this concept to deep learning, showing that training data from deep neural networks could also be reconstructed.

Current MIA techniques in collaborative inference can be broadly categorized into Maximum Likelihood Estimation-based (MLE-based) MIAs and Generative Model-based (Gen-based) MIAs, which are further analyzed in the following sections.

**MLE-based MIAs.** MLE-based MIA originated from the 2015 study by Fredrikson et al. [12], which reconstructed training data from a multilayer perceptron (MLP). This method minimizes the difference between target and output class confidence scores as a loss function and employs gradient descent to optimize the input, enabling the reconstruction of the original training data. Subsequent research enhanced this approach by incorporating techniques like Total Variation (TV) [37] loss as a regularization term to improve optimization, with these improved methods later referred to as rMLE-based MIA by He et al. [19] In collaborative inference scenarios, MLE-based methods are particularly effective for reconstructing data from shallow neural networks deployed on edge

devices. Unlike the prediction vectors produced by full neural networks, the richer feature representations and lower complexity of shallow networks provide adversaries with more detailed and easily optimizable gradient information.

**Gen-based MIAs.** This method originated from the 2019 work of Yang et al. [51], who reconstructed input data in facial recognition systems by using generative deep learning models  $g$  to approximate the inverse mapping function of the target model  $f^{-1}$ , such that  $g \approx f^{-1}$ . By inputting prediction vectors into  $g$ , they successfully generated facial input images. Building on this approach, He et al. [19] extended it to collaborative inference scenarios, demonstrating that input data from edge models is more vulnerable to reconstruction, thereby highlighting the risks associated with collaborative inference. Unlike MLE-based methods, Gen-based MIA does not require white-box access to the edge model. Instead, it trains the attack model by calculating losses based on transmitted features, enabling it to approximate the inverse mapping of non-linear computations. Furthermore, as edge models in collaborative inference are typically shallow neural networks, their outputs often retain redundant information from the original input and features, maintaining a strong correlation between inputs and outputs and facilitating the reconstruction process.

## 2.3 Related defense work

To protect the input data collected by edge devices in collaborative inference from potential leakage, He et al. [19, 20] highlighted the necessity of developing defense strategies while identifying these threats. Building on a detailed analysis of attack methods, subsequent defense techniques have gradually evolved in recent years. These defenses can be broadly categorized into three types: perturbation-based defenses, information bottleneck-based defenses, and defenses combining neural network depth with information bottleneck principles. The following sections provide a detailed overview of each of these defense strategies.

**Perturbation-based defense.** This approach introduces carefully designed noise perturbations into the gradients and output features of the edge model during training to reduce the likelihood of adversaries extracting meaningful information and defend against MIA. He et al. [20] initially proposed using Gaussian noise and random feature dropout to limit the effective information accessible to attackers, and later, Wang et al. [46] extended this strategy by dynamically adjusting the depth of the edge model while adding differential privacy noise to transmitted features. Although these methods enhance defenses, they significantly impact model usability, often reducing accuracy by approximately 10%, and remain less effective against Gen-based MIA. This is because sufficiently expressive decoders in attack models can adapt to small noise or feature dropout, leveraging reconstruction capabilities similar to denoising auto-encoders (DAE) [14], potentially increasing attack robustness. In centralized MIA defenses, Struppek et al. [43] proposed perturbing training labels by setting the label smoothing factor to a negative value, which significantly reduced the effectiveness of MLE-based MIA and offers an alternative perspective for designing defense strategies.

**IB-based defense.** This approach enhances defenses against inference attacks by limiting the mutual information between input

data  $x$  and intermediate features  $z$  while preserving the mutual information between features and outputs  $y$ , thereby maintaining predictive performance [45]. The objective of this defense can be formally expressed as follows:

$$\min_{\theta} -I(z, y) + I(x, z) \quad (2)$$

Initially, Wang et al. [45] introduced information bottleneck theory into MIA defenses, but their method was not optimized for collaborative inference and required substantial computational resources when applied to intermediate features. To address this, Peng et al. [34] proposed BiDO (Bilateral Dependency Optimization), which optimizes the correlation between inputs, features, and outputs using dependency algorithms. BiDO reduces the correlation between inputs and features while strengthening the correlation between features and outputs, balancing defense and performance. Additionally, Wang et al. [47] and Duan et al. [10] explored direct mutual information estimation between inputs and features using methods based on mutual information definitions and the CLUB (Contrastive Log Upper Bound) [5] technique, incorporating the estimates as constraints in the optimization objective. IB-based defenses provide interpretable protection mechanisms and valuable design insights for future research. However, these methods face limitations: BiDO relies on kernel functions to constrain nonlinear correlations, and its performance is highly sensitive to hyper-parameter choices, such as kernel bandwidth. Poor parameter selection can result in suboptimal optimization. Methods based on mutual information definitions are constrained by sample scale to estimate  $I(x, z)$ .

**NND & IB-based defenses.** Building on the natural advantages of deep neural networks in resisting inference attacks and incorporating information bottleneck theory, this approach designs targeted loss functions to further enhance defense effectiveness. Building on this, Ding et al. [8] proposed increasing network depth while compressing newly added hidden layers to restrict the transmission of redundant information. Subsequently, Azizian et al. [3] proposed an improved defense method by introducing encoders at the edge and decoders at the cloud, forming an auto-encoder (AE) structure. The encoder at the edge increases network depth and reduces feature dimensionality, achieving the information bottleneck effect, while the decoder at the cloud restores information to maintain predictive performance. Additionally, an  $l_1$ -norm constraint is applied during feature transmission to reduce attack risks, and adversarial training is used to enhance defense resilience against inference attacks.

However, this class of methods has certain limitations. First, increasing the depth of neural networks and adding additional modules inevitably raises computational overhead and hardware requirements on edge devices, limiting the method's applicability. Second, the introduction of adversarial training not only obscures certain aspects of the original defense strategy's effectiveness but also introduces additional challenges. It is less effective against future, more advanced attacks, increases the difficulty of fine-tuning edge models, and may degrade inference performance [54]. Additionally, adversaries can adapt their attack models using similar adversarial strategies, reducing the overall effectiveness of the defense [25]. Thus, while these methods enhance defense performance,

their implementation requires careful consideration of computational resources, model adaptability, and suitability for specific application scenarios.

### 3 THREAT MODEL

#### 3.1 Knowledge background of adversary

**Attack scenarios.** Based on the adversary's level of knowledge, attack scenarios can be categorized into the following three types:

- (1) **White-box Scenario:** The adversary has complete white-box knowledge of the edge model, including its architecture, parameters, and gradient information.
- (2) **Black-box Scenario:** The adversary has only black-box access to the model, restricting their capability to observing the intermediate features. Additionally, their understanding of the edge model's architecture is restricted to prior knowledge or incomplete assumptions.
- (3) **Gray-box Scenario:** The adversary has partial knowledge of the edge model's architecture but remains unaware of defensive modifications, such as increased depth or additional hidden layers.

The gray-box scenario enables the adversary to leverage their partial understanding of the edge model's architecture to enhance the capability of their inversion model. For instance, if the defender partitions the first three convolutional layers of a ResNet-18 model [18] and further deepens the network, while the adversary is only aware of the original ResNet-18 architecture, the adversary can only construct an approximate attack model based on partial knowledge of the initial layers. However, in the gray-box scenario, the adversary can address this limitation by utilizing their understanding of the edge model's architecture and reasoning about its mapping capabilities to refine their inversion model.

#### Knowledge shared by adversaries in different scenarios.

First, in attack scenarios, the adversary is assumed to understand the edge model's core task. To enhance their capability, the attack model in Gen-based MIA is trained on data distributions closely matching the target distribution, as detailed in Section 6. Second, the adversary has access to lossless transmission features and their dimensional distribution, which are essential for attacks, as the features represent high-dimensional input data and the distribution informs the design of the attack model.

This study focuses on image classification tasks, though the proposed defense methods extend to other tasks where the edge model primarily performs feature extraction. Tasks like segmentation, detection, and classification rely on convolutional layers for shallow feature extraction, with task-specific variations having minimal impact on reconstruction objectives. Prior work [3] has also demonstrated input reconstruction effectiveness in object detection using Gen-based MIA.

Moreover, image data, due to its high dimensionality, is especially vulnerable to MIA attacks, as shallow convolutional layers retain redundant information [18, 56]. This makes defenses in image-based tasks more demonstrable. In contrast, textual data, with its strong contextual dependencies and syntactic complexity, has shown limited success in existing researches for achieving high-quality MIA reconstructions [7, 55]. This work focuses on image data to explore privacy-preserving techniques, leveraging its interpretability and

the intuitive nature of defense effectiveness to validate the proposed methods.

### 3.2 Attack strategy of the adversary

In the white-box attack scenario, the adversary can perform attacks using the rMLE-based MIA method proposed in [19, 20]. To ensure the experiments are both comparative and representative, hyperparameter adjustments were made to achieve performance closer to optimal.

In the black-box attack scenario, the adversary can employ methods from [19, 51, 52], relying solely on output features for reverse mapping without access to the edge model's internal details. When protected by NND & IB-based defenses, the adversary lacks knowledge of architectural changes and must design the attack model based on prior assumptions.

In the gray-box attack scenario, the adversary can employ black-box strategies while leveraging known architectural information to optimize the attack model. This allows the reverse mapping capability to adapt to changes in the edge model. Detailed designs and training procedures for the attack models are provided in Section 6.

## 4 THEORETICAL ANALYSIS OF MIA IN CI

This section analyzes key factors affecting MIA effectiveness in collaborative inference, introduces a formulaic representation of its principles, and establishes a difficulty criterion from an information-theoretic perspective. We validate this criterion through experiments and use it to guide the design of SiftFunnel.

### 4.1 Principles analysis of MIA

MIAs are categorized into MLE-based and Gen-based methods, both aiming to reconstruct input data using the target model's output. MLE-based MIA calculates the loss between transmitted features and the edge model's output, then iteratively applies gradient descent to optimize the input, achieving reconstruction of the original data. The attack principle is formulated as follows:

$$\begin{aligned} x^{(k+1)} &= x^{(k)} - \eta \nabla_x \mathcal{L}(x, f_{\text{edge}}(x^{(k)}), z), \\ x^* &= \arg \min_x \mathcal{L}(x, f_{\text{edge}}(x^{(k)}), z) \end{aligned} \quad (3)$$

Where  $x^{(k)}$  represents the input value at the  $k$ -th iteration, typically initialized as Gaussian noise, zeros, or ones.  $x^*$  denotes the final reconstructed result,  $z$  represents the transmitted features of the target input.  $f_{\text{edge}}(\cdot)$  refers to the target edge model,  $\nabla_x \mathcal{L}$  is the gradient calculated from the loss function and edge model parameters to optimize  $x$ , and  $\eta$  is the step size for each update.

According to [19], the loss function combines the  $l_2$  distance between  $f_{\text{edge}}(x^{(k)})$  and  $z$  with a TV regularization term for  $x$ , forming the basis of rMLE-based MIA. The method relies on gradient descent, where the loss values depend on output features and gradients are computed using the target model's parameters.

To achieve effective attacks, sufficient output feature information  $\delta(z)$  and a well-chosen loss function are essential to ensure optimization space. Additionally, white-box knowledge of the edge model is required, as complex model mappings and limited feature information increase the risk of gradient descent converging to

local minima [42, 56]. For instance, if two similar images produce nearly indistinguishable output features, reconstruction becomes challenging.

When dealing with complex edge model mappings or models protected by defense techniques, directly computing gradients in MLE-based MIA can significantly hinder optimization performance. To address this, He et al. [19, 20], building on the method from [51], developed a reverse mapping network for the edge model, which is categorized as Gen-based MIA. The key idea is to use a generator to approximate the reverse mapping of the edge model, achieving  $\text{Data} \approx \text{Generator}(\text{Feature})$ . Different methods adopt various strategies to train the generator. For instance, Yang et al. [51] trained a decoder using auxiliary task-related datasets, while Yin et al. [52] utilized intercepted feature data for training. The principle of this attack is summarized as follows.

$$\begin{aligned} G &= \arg \min_G \mathbb{E}_{x' \sim p(x')} \mathcal{L}(G(f_{\text{edge}}(x')), x'), \\ x^* &= G(z) \end{aligned} \quad (4)$$

Where  $x'$  represents samples from an auxiliary data distribution  $p(x')$ . The loss function, typically MSE, measures the distance between  $x'$  and the reconstructed data  $G(f_{\text{edge}}(x'))$  or  $z = f_{\text{edge}}(x')$ . The trained generator  $G$  must achieve the desired mapping  $G \approx f_{\text{edge}}^{-1}$  to reconstruct  $x^*$ .

The above formula highlights the conditions required for effective attacks:

- (1) A well-matched training dataset aligned with the target task, ideally with a distribution similar to the target dataset [51].
- (2) Sufficient and highly separable input information for the generator.

The rationale is that if the information in  $f_{\text{edge}}(x')$  is insufficient or cannot independently represent  $x'$ 's features, the loss in (4) will struggle to converge as  $G(f_{\text{edge}}(x'))$  remains ambiguous, limiting its training. These conditions must be met simultaneously. For instance, even with random feature drops, if the remaining features effectively distinguish inputs, the attack can still achieve satisfactory reconstruction [20]. Such frameworks resemble DAE [14], where the decoder can adapt to noise or feature drops.

Gen-based MIA demonstrates superior reconstruction performance compared to MLE-based MIA in defense scenarios. First, it avoids relying on model parameters for gradient computation, eliminating challenges from non-convex optimization. Second, it depends only on edge model output, offering greater flexibility. Furthermore, existing defenses struggle to effectively remove redundant feature information, allowing Gen-based MIA to overcome defenses if the generator is capable of learning the edge model's reverse mapping.

### 4.2 Difficulty criterion for MIA in CI

Above, we summarized the factors influencing MIA effectiveness through a formulaic representation of its principles. However, this alone does not provide a concrete basis for evaluating the difficulty of implementing MIA. To address this, we will formalize and analyze these factors from an information-theoretic perspective to establish a clear criterion.

First, the mutual information between the input  $x$  and the feature  $z$ ,  $I(x; z)$ , can be expressed as:

$$I(x; z) = H(x) - H(x | z) = H(z) - H(z | x) = H(z) \quad (5)$$

Where  $H(x | z)$  represents the conditional entropy of input  $x$  given  $z$ , and  $H(z | x)$  represents the reverse. Since there is no uncertainty in the mapping from  $x$  to  $z$  through  $f_{\text{edge}}$ ,  $H(z | x)$  is zero.

From Equation (5), we observe that complex mappings and information loss during neural network transmission reduce  $I(x; z)$  and increase  $H(x|z)$ , making non-convex optimization more difficult. Consequently, this increases the challenge for MLE-based MIA to reconstruct  $x$  from  $z$ .

An inappropriate loss function or insufficient output information can further increase  $H(x|z)$  and decrease  $H(z)$ . It is important to note that a low  $\delta(z)$  does not necessarily imply a low  $H(z)$ . For instance, even if 80% of  $z$ 's elements are randomly dropped,  $H(z)$  could remain high, as small amounts of information can still exhibit high entropy [20]. Therefore, the performance of MLE-based MIA is directly influenced by  $H(x|z)$ ,  $H(z)$ , and  $\delta(z)$ .

To further illustrate the influence of mutual information and entropy on the difficulty of MIA, we can derive the following relationship for any  $x \rightarrow z \rightarrow x^*$  using Fano's inequality [2, 49]:

$$H(P_e) + P_e \log |\mathbb{X}| \geq H(x | x^*) \geq H(x | z) \quad (6)$$

where  $P_e = \text{Prob}\{x \neq x^*\}$ ,  $x^*$  is the reconstruction by MIA, and  $\mathbb{X}$  denotes the value space of  $x$ .

Since  $\mathbb{X} \geq 2$  and  $H(P_e) \leq 1$ . Therefore inequality (6) can be written as

$$P_e \geq \frac{H(x | z) - 1}{\log |\mathbb{X}|} = \frac{H(x) - I(x, z) - 1}{\log |\mathbb{X}|} = \frac{H(x) - H(z) - 1}{\log |\mathbb{X}|} \quad (7)$$

Since  $H(x)$  and  $|\mathbb{X}|$  are influenced by training data, they are typically assumed to be objective and invariant. Therefore, through inequality (7), we observe that increasing the lower bound of  $P_e$ , and thus the difficulty of MIA, is influenced by  $H(x|z)$ ,  $H(z)$ , and  $I(x, z)$ .

From Equation (4), Gen-based MIA requires sufficient input information  $\delta(z)$  and high  $H(z)$  to ensure maximum separability and enable loss convergence, allowing the generator to simulate reverse mapping effectively. Notably,  $\delta(z)$  and  $H(z)$  are not directly proportional, as high average information does not always guarantee separability. A larger  $\delta(z)$  not only facilitates generator training but also directly impacts the reconstruction of  $x^*$ . The relationship in Inequality (7) is also applicable here.

The validity of related research can also be explained by both. For example, [51] reduces  $\delta(z)$  by pruning output information, disrupting training and reconstruction, while [57] increases entropy via nonlinear functions to enhance generator performance. Thus,  $H(z)$  and  $\delta(z)$  are critical factors influencing Gen-based MIA.

The analysis indicates that the difficulty of implementing both types of attacks is inversely proportional to mutual information, entropy, and the amount of information. The difficulty of MIA can be formulated as follows, where  $k_1$  and  $k_2$  are proportionality constants.

$$D_{\text{mia}} \propto \left( \frac{k_1}{\{I(x; z); H(x | z); H(z)\}} + \frac{k_2}{\delta(z)} \right) \quad (8)$$

Based on this criterion, existing defenses [10, 34, 45] using the information bottleneck theory can be understood as approximating a reduction in  $I(x; z)$  through various algorithms to increase the difficulty of MIA. Perturbation-based defenses [20] aim to directly increase  $H(x|z)$ . The defensive effect of deeper neural networks [3, 8] can be explained by their ability to reduce  $I(x; z)$  and  $\delta(z)$ .

This is primarily because, without skip connections [17], mutual information decreases progressively during the forward propagation in neural networks. In contrast, residual networks with skip connections add the output of one layer to its input, which may prevent  $\delta(z)$  from decreasing and, in some cases, even cause it to increase.

### 4.3 Experimental Demonstration of the Criterion and Guidance for Defense Design

To validate  $D_{\text{mia}}$  and the theoretical analysis, we designed experiments using a CNN that progressively reduces spatial size while increasing channel size, based on the framework in [18, 51], and ResNet-18 with skip connections, quantifying each block. We trained MINE [4] on the same dataset used to train the full model  $f$  to estimate the lower bound of mutual information. The core idea of MINE is to optimize a neural network estimator using the Donsker-Varadhan representation (DV bound) [9] as the loss function, providing an approximate estimate of the mutual information between random variables.

Mutual information is defined as follows:

$$I(X; Z) = \mathbb{E}_{p(x,z)} \left[ \log \frac{p(x,z)}{p(x)p(z)} \right] \quad (9)$$

Where  $p(x, z)$  represents the joint distribution, existing defense methods approximate it, but limited batch sizes lead to inaccuracies and variations in mutual information estimates. For high-dimensional data (e.g., images), accurate estimation requires many samples.

To avoid direct distribution estimation, the Donsker-Varadhan representation reformulates mutual information as an optimization problem:

$$I(X; Z) \geq \sup_T \mathbb{E}_{p(x,z)} [T(x, z)] - \log \mathbb{E}_{p(x)p(z)} \left[ e^{T(x,z)} \right] \quad (10)$$

Where  $T$  is a learnable function, this formulation enables mutual information to be estimated by optimizing  $T$  to obtain a lower bound.

MINE achieves this by parameterizing  $T$  with a neural network  $T_\theta$  and maximizing the DV bound through gradient descent to approximate mutual information:

$$\hat{I}(X; Z) = \mathbb{E}_{p(x,z)} [T_\theta(x, z)] - \log \mathbb{E}_{p(x)p(z)} \left[ e^{T_\theta(x,z)} \right] \quad (11)$$

As shown in Figure 2, we trained target models on the CIFAR-10 [26] and used Equation (11) to train MINE for the corresponding blocks. Figures 2(a, b) show that increasing network depth reduces both mutual information and effective information, leading to a decline in attack performance. Figures 2(c, d) illustrate that while skip connections within two layers do not reduce effective information, they slightly lower mutual information, moderately affecting attack performance.

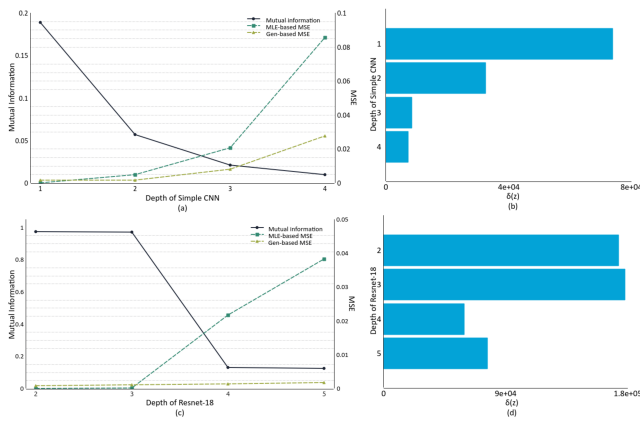


**Figure 2: The impact of neural network depth on  $I(x, z)$ ,  $\delta(z)$ , as well as MLE & Gen-based MIA.**

Previous research [17] identified vulnerabilities caused by skip connections in centralized MIA. Our study further highlights their impact on MIA effectiveness in collaborative inference. Transmission between layers alters feature channels and dimensions, requiring a shortcut layer, which leads to a more pronounced decline in mutual information compared to direct stacking within layers. This, in turn, degrades MIA performance and aligns with our criterion.

Notably, while mutual information at ResNet’s fourth layer is higher than that at CNN’s second layer, MLE-based MIA does not perform better. This is because these methods rely heavily on gradient descent, making them sensitive to suboptimal optimizers, hyper-parameter settings, and deeper network structures, which hinder gradient calculations for optimizing  $x$ . The lack of flexible and efficient methods for MLE-based MIA remains a gap in current research, often leading to their exclusion in defense evaluations—a topic warranting further exploration [8].

In our experiments, we still evaluate MLE-based MIA against various defenses and provide evidence demonstrating the effectiveness of our method in defending against such attacks.

In conclusion, through theoretical analysis and experimental validation, we established  $D_{mia}$  and determined that effective defense strategies must impact mutual information, entropy, and  $\delta(z)$ . The following considerations should guide defense design:

- Since  $I(x, z)$  is challenging to compute and current algorithms lack flexibility and efficiency, defenses should focus on indirectly influencing  $H(x | z)$  and  $H(z)$ .
- The design of edge models should strategically affect  $H(z)$  and  $\delta(z)$ .
- For practical applications, the light-weighting of edge models should balance usability with their impact on the factors outlined in the criterion.

## 5 SIFTFUNNEL: INFORMATION SIFTING FUNNEL

Building on the theoretical analysis, criterion, and experiments in Section 4, this section introduces SiftFunnel and its adherence to  $D_{mia}$  in edge model and loss function design.

We first outline the core principles and objectives of SiftFunnel. Then, we detail the edge model’s structure, key modules, and role in the forward propagation of information. Finally, we explain the loss function’s impact on  $H(x | z)$ ,  $H(z)$  and  $\delta(z)$ , highlighting its ability to extract useful information while minimizing redundancy.

### 5.1 Overview of SiftFunnel

Guided by  $D_{mia}$ , SiftFunnel aims to balance usability and privacy in edge models by increasing the uncertainty of inferring  $x$  from  $z$  while reducing  $z$ ’s information content and separability. To this end, as shown in Figure 3, we introduce two key improvements: First, the edge model is enhanced by modifying the final hidden layer into a funnel-shaped structure and incorporating attention mechanism modules between layers. Second, the loss function is optimized to ensure that model training balances usability with privacy protection.

Specifically, in the edge model design, the final layer adopts a funnel-shaped structure, reducing feature channels while preserving spatial dimensions. This reduces computation, lightens the edge device load, and limits redundant information. Attention mechanisms and multi-receptive field convolutions enhance task-relevant information, while a feature channel supplementation module in the cloud model ensures task accuracy. With the improved edge model, designing an effective loss function is essential. To reduce redundancy and mutual information between  $z$  and  $x$ , we use Distance Correlation [27] for nonlinear correlations and the Pearson Coefficient [6] with  $l_1$ -norm for linear correlations. Additionally, label smoothing and KL divergence [9] ensure model accuracy, enhancing usability while reducing the separability of  $z$ .

### 5.2 The Design of Shallow Edge Model

**Information Funnel.** Deepening the neural network enhances feature extraction and reduces  $I(x, z)$ , as confirmed in the Section 4. Previous work [21] also demonstrates through Fisher information [36] that deeper networks improve feature relevance to tasks. Inspired by this, we redesign the final layer of the edge model with an Information Funnel module. This module reduces output channels to one-fourth in the first layer and further in the second layer, with channel selection based on the spatial size of feature maps. If the spatial size is reduced significantly, channels can exceed 10 to maintain accuracy. If unchanged, channels can be set to 2 to limit redundancy while preserving accuracy. Adjusting channels based on spatial size is necessary because spatial information loss is irreversible, whereas channel information loss can be compensated in the cloud model. While this compensation increases  $I(z, y)$ , it does not reverse the reduction in  $I(x, z)$ , ensuring attack difficulty remains high, as demonstrated in Section 6.3. So, we add the channel compensation module in the cloud model to guarantee usability. Notably, assumption about extracting features from non-independent transmission modules is extremely strong and idealized, requiring the adversary to have full white-box knowledge of the cloud model as if they were the developer.

The Information Funnel’s channel structure controls output but does not limit redundancy or enhance task-relevant information transmission, affecting usability. Inspired by Inception networks [44], we redesign it as a multi-receptive field convolutional



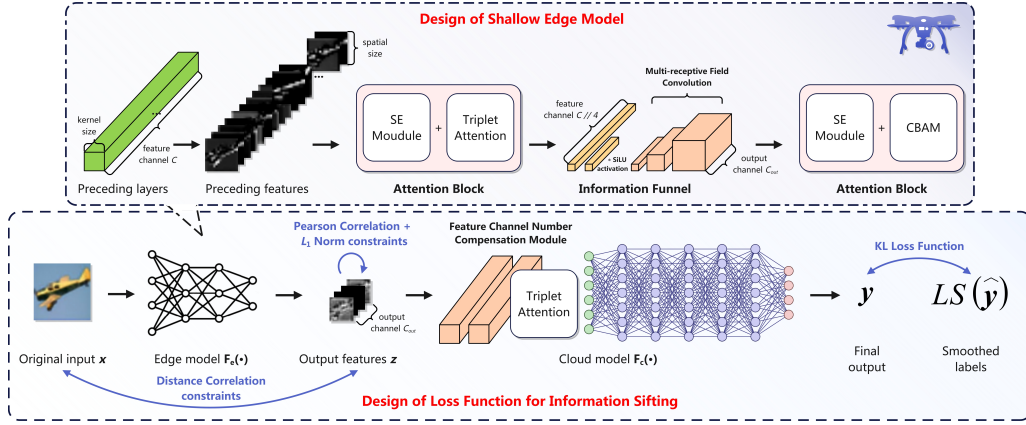


**Figure 3: Overview of SiftFunnel. Specifically, the design is divided into two aspects: the architecture and the loss function for the edge and cloud model.**

framework with three low-channel layers. A  $1 * 1$  kernel fuses channel information, followed by  $3 * 3$  and  $5 * 5$  kernels to expand the receptive field, extract richer task-relevant features, improve decision-making, and reduce mutual information with  $x$ , while lowering parameters of the edge model and controlling  $\delta(z)$ .

**Attention Block.** To enhance the output of task-relevant information from the Information Funnel, attention mechanism modules are added both before and after it. The first module combines an SE block [23] and Triplet Attention [32]. The SE block evaluates the contribution of information within each channel, suppressing or nullifying channels with low task relevance. Triplet Attention reduces spatial information while maintaining smooth and continuous outputs, preserving fine-grained features suitable for further processing. The second attention mechanism integrates SE and CBAM modules [48]. Compared to Triplet Attention, CBAM is a more lightweight module that sequentially calculates channel and spatial weights to enhance or suppress input features, improving network performance. Since CBAM’s channel and spatial attention are independently designed, certain regions are suppressed redundantly, making the output features more sparse. This is ideal for final output processing, effectively increasing  $H(x|z)$  while suppressing  $H(z)$  and  $\delta(z)$ .

### 5.3 The Design of Loss Function

To further enhance model usability and data privacy, a appropriately designed loss function is essential to guide the training process.

To reasonably increase  $H(x|z)$  and suppress  $H(z)$  within the edge model structure—thereby increasing the uncertainty of inferring  $x$  from  $z$ —loss constraints must be applied to  $x$  and  $z$ . The key challenge is that, without intervention, neural networks may retain irrelevant input information in their output during forward propagation. This information, which does not significantly impact decision-making, reduces the difficulty of attacks by maintaining  $I(x, z)$ .

Some defense approaches utilize Constrained Covariance (COCO) [16] to estimate correlation, focusing primarily on the linear relationship between  $x$  and  $z$ . However, since neural networks predominantly perform nonlinear operations, studies have shown that

this constraint is not only ineffective but may also lead to reduced accuracy [34]. Alternatively, some approaches employ the Hilbert-Schmidt Independency Criterion (HSIC) [15] to estimate correlation. However, kernel-based calculations in HSIC rely heavily on the appropriate selection of  $\sigma$ . Improper  $\sigma$  value can introduce bias in nonlinear correlation estimation, limiting the generalizability of this method and reducing its effectiveness across various scenarios.

**Nonlinear correlation constraint.** We observe that shallow neural network features retain significant similarity to the input and are derived through nonlinear operations. To address this, we use distance correlation to measure the nonlinear relationship between  $x$  and  $z$ , incorporating it as a loss constraint. This helps remove redundant input information from the output, effectively increasing  $H(x|z)$ . The calculation of distance correlation is as follows:

$$\mathcal{L}_{dCor} = dCor(x, z) = \frac{dCov(x, z)}{\sqrt{dVar(x) \cdot dVar(z)}} \quad (12)$$

Where  $dCov(x, z)$  represents the distance covariance between  $x$  and  $z$ , and the denominator is the product of the distance variances for the two datasets.

To compute the numerator, a distance matrix  $A$  is first calculated, where each element is the Euclidean distance between samples, defined as  $A = \|x_i - x_j\|_2$ . To remove the influence of sample shifts, the distance matrix is centered as  $A_{ij}^c = A_{ij} - \bar{A}_i - \bar{A}_j + \bar{A}$ , where  $\bar{A}_i$  denotes the mean of the  $i$ -th column, and similar operations apply to other terms. With the centered distance matrix, the distance covariance is computed as  $dCov(x, z) = \frac{1}{n^2} \sum_{i,j} A_{ij}^c B_{ij}^c$ , where  $B$  represents the matrix of features  $z$ , and  $n$  denotes the batch size.

The distance variances is defined as  $dVar(x) = \frac{1}{n^2} \sum_{i,j} A_{ij}^c{}^2$ , which normalizes the distance covariance. The value range of distance correlation is  $[0, 1]$ , where 1 indicates perfect correlation. Since  $x$  and  $z$  exhibit high distance similarity and are derived through nonlinear operations, distance correlation is well-suited as a constraint term. Moreover, as a distribution-free measure, it does not rely on specific data distributions, making it effective for non-Gaussian distributions, nonlinear relationships, and complex data types such as images and text. For non-stationary and

multimodal data, distance correlation provides stable dependency measurements, allowing the constraint to flexibly adapt to different models and datasets.

**Linear correlation constraint.** In addition to constraining the loss between  $x$  and  $z$ , it is necessary to design loss constraints specifically for the  $z$ . The primary issue lies in the  $z$  containing repetitive or similar information, which is redundant for decision-making and provide additional input for Gen-based MIAs, strengthening local constraints in the input space and improving reconstruction accuracy.

To address this, we propose using the Pearson correlation coefficient as a loss constraint to reduce the linear correlation within features  $z$ , effectively eliminating redundant information. The calculation is as follows:

$$\mathcal{L}_{\text{Pearson}} = \frac{1}{C^2} \sum_{c_1=1}^C \sum_{c_2=1}^C (\text{pCor}_{c_1, c_2})^2 = \frac{1}{C^2} \sum_{c_1=1}^C \sum_{c_2=1}^C \left( \frac{\text{Cov}_{c_1, c_2}}{\sigma_{c_1} \cdot \sigma_{c_2}} \right)^2 \quad (13)$$

Where  $\text{Cov}_{c_1, c_2}$  represents the covariance matrix between channels  $c_1$  and  $c_2$ , calculated as  $\text{Cov}_{c_1, c_2} = \frac{1}{H \cdot W} \sum_{i=1}^{H \cdot W} (z_{c_1, i} - \mu_{c_1}) \cdot (z_{c_2, i} - \mu_{c_2})$ , where  $z_{c_1, i}$  is the  $i$ -th element of channel  $c_1$  and  $\mu_{c_1}$  is its mean.  $H$  and  $W$  denote the height and width of the feature space.  $\sigma_{c_1}$  and  $\sigma_{c_2}$  are the standard deviations, calculated as  $\sigma_{c_1} = \sqrt{\frac{1}{H \cdot W} \sum_{i=1}^{H \cdot W} (z_{c_1, i} - \mu_{c_1})^2}$

To compute the scalar  $\mathcal{L}_{\text{Pearson}}$ , the squared correlations of all channel pairs are averaged, keeping the value range within  $[0, 1]$ . This avoids negative values, which could lead to suboptimal updates during gradient descent. Minimizing the  $\mathcal{L}_{\text{Pearson}}$  in the presence of negative values might push the correlation toward complete negative correlation, introducing unnecessary feature redundancy or unsuitable learning patterns, ultimately preventing convergence. Therefore, the goal is to minimize the coefficient toward zero, as lower values indicate reduced linear correlation. Using the squared correlations and their average ensures a smoother and more stable gradient descent process.

Additionally, to prevent extreme values in the feature output weights during the optimization of the above constraints, we include the  $l_1$ -norm as a loss term. This term is added specifically to suppress weights, but excessive emphasis on it could interfere with normal model training. Therefore, the coefficient  $\tau$  for this loss term is set below  $1e-2$  to balance its influence.

**Label smoothing.** Finally, to ensure model accuracy, we draw inspiration from [43] and apply label smoothing to refine the target loss, as shown in the formula (14). Additionally, KL divergence is used instead of cross-entropy (CE) as the primary loss function for optimization.

$$LS(\hat{y}_c) = 1 - \alpha + \frac{\alpha}{K}, \quad LS(\hat{y}_i) = \frac{\alpha}{K} \quad (14)$$

Where  $LS(\hat{y}_c)$  refers to the label smoothing element under the target class,  $LS(\hat{y}_i)$  is the  $i$ -th element of the non-target class.  $\alpha$  is smooth factor and  $K$  is the total number of categories.

This smoothing mechanism ensures that the loss value computed by cross-entropy emphasizes enhancing inter-class feature distinctions, while KL divergence as a loss function supports smoother and

more generalized feature extraction between classes [43]. Within-class feature extraction focuses on capturing universal characteristics, ensuring the model maintains a certain level of generalization and robustness for the target task. Moreover, this optimization reduces maximum feature separability, increasing the difficulty of attacks, as demonstrated in Section 6.

In summary, the proposed loss function first applies nonlinear correlation constraints between input  $x$  and features  $z$  to increase  $H(x | z)$  and suppress  $H(z)$ . Second, it imposes linear correlation and extreme value constraints on  $z$  to further enhance  $H(x | z)$  and suppress  $\delta(z)$ . Finally, label smoothing is applied to the target loss to maintain accuracy while slightly suppressing  $H(z)$ . The final formulation of this optimization is as follows, with specific parameter settings referenced in Section 6.

$$\min \mathcal{L}_\theta(x, z, \hat{y}) = \lambda_1 \cdot KL(f(x), LS(\hat{y})) + \lambda_2 \cdot \mathcal{L}_{\text{dCor}} + \lambda_3 \cdot \mathcal{L}_{\text{Pearson}} + \tau \cdot \|z\|_1 \quad (15)$$

## 6 EXPERIMENTS

In this section, we systematically evaluate the resistance to MIA and compare our method with existing approaches. The results are analyzed from three perspectives: the impact of defense methods on  $I(x | z)$  and  $\delta(z)$ , the influence of datasets and model architectures, and ablation studies. The specific experimental setup and evaluation metrics are shown below.

### 6.1 Experimental Setup

1) *Datasets.* We used three types of image recognition datasets, with processing details outlined as follows. The detailed data allocation is shown in Table 1.

- **CIFAR-10** [26]. The CIFAR-10 dataset consists of 60,000 RGB images categorized into ten classes (e.g., airplane, ship, etc.) with an original resolution of  $32 \times 32$ . To make the results clearer and more intuitive, we used an upscaled resolution of  $64 \times 64$ .
- **FaceScrub** [33]. FaceScrub is a URL dataset with 100,000 images of 530 actors, which contains 265 male actors and 265 female actors. However, since not every URL was available during the writing period, we downloaded a total of 43,149 images for 530 individuals and resized the images to  $64 \times 64$ .
- **CelebA** [29]. CelebA is a dataset with 202,599 images of 10,177 celebrities from the Internet. We used the same crop as [51] to remove the background of images in this dataset other than faces to reduce the impact on the experiment. In order to eliminate individual overlap, we removed a total of 6,878 images of 296 individuals from CelebA and similarly resized the images to  $64 \times 64$ .
- **ChestX-ray** [38]. This dataset is a curated collection of COVID-19 chest X-ray images compiled from 15 publicly available datasets. It contains 1,281 COVID-19 X-rays, 3,270 normal X-rays, 1,656 viral pneumonia X-rays, and 3,001 bacterial pneumonia X-rays. For our analysis, we converted the images to gray scale with a resolution of  $128 \times 128$ .

2) *Attack Method.* The selection of attack methods has been discussed in Section 3.2. Specifically, for MLE-based MIA, this paper has adjusted to the hyperparameter values that yield the best results.

**Table 1: Data allocation of the target model and attack model.**

Classifier		Attack Model
Task	Data	Auxiliary Data
CIFAR-10 (10 classes)	Train: 66.6%, Test: 16.7%	16.7% (10 classes of CIFAR-10)
FaceScrub (530 classes)	Train: 80%, Test: 20%	CelebA (non-individual overlapping)
ChestX-ray (4 classes)	Train: 66.6%, Test: 16.7%	16.7% (4 classes of ChestX-ray)

For Gen-based MIA, the attack model in this paper is designed as the inverse architecture of the edge model. Moreover, under the gray-box scenario assumption, the attack model can enhance the expressive power of the reverse mapping as the edge model architecture changes. The attack model is also trained using the Adam optimizer with a learning rate of  $2e-4$ , a  $\beta_1$  of 0.5, and a ReduceLRonPlateau scheduler with a factor of 0.5 and patience of 20. The training conditions for the attack models in this paper have been done with strong assumptions and only the attack models where the test Mean Square Error (MSE) reaches the minimum value are saved to highlight the effectiveness of the defense efforts.

3) *Target Edge Model and Implementation Details.* We employ the same comprehensive model architecture as detailed in [51], comprising four Convolutional Neural Network (CNN) blocks succeeded by two fully connected layers. This model is trained using the Adam optimizer with a learning rate of  $2e-4$ , a  $\beta_1$  parameter of 0.5, and a ReduceLRonPlateau scheduler with a reduction factor of 0.5 and a patience setting of 25. Each CNN block is composed of a convolutional layer, a batch normalization layer, a max-pooling layer, and a ReLU activation function. The target edge model encompasses the initial two CNN blocks. For the training of the edge model protected by SiftFunnel, we have specified the parameters  $\alpha$  to 3.5,  $\epsilon$  to 0.35,  $\beta$  to 0.8, and  $\gamma$  to 0.6 in Equation (15). In addition to this, to argue the impact of the model architecture for the defense, we use different CNNs as follows: (1) VGG16 adapted from [41]; (2) ResNet-18 adapted from [18], the learning rates are  $3e-4$ . The division positions of resnet and vgg are not fixed. For detailed accuracy and how to divide them, see Section 6.3 for analysis. All experiments were performed on two RTX 4090 GPUs and an Intel Core i9-14900KF  $\times$ 32 CPU.

4) *Comparison of Defense Methods.* We will compare three existing categories of defense methods. For Perturbation-based defenses, we select **Adding noise & Dropping features** [20], **DPSGD** [1], and **negative label smoothing (NLS)** [43]. For IB-based defenses, we choose **MID** [45], **BiDO** (with HSIC) [34], **VIB** [47], and **InfoSCISSORS** [10]. For NND & IB-based defenses, we opt for **AE-based protection** [3]. Our method falls into the NND & IB-based defense category, which also requires analyzing the defensive effect in a gray-box scenario. Furthermore, all comparison methods have been selected and set with appropriate hyper-parameters for comparison, with detailed settings found in Section 6.3 analysis. Lastly, all methods are trained without adversarial training, focusing solely on the effects of the original defense methods.

## 6.2 Evaluation Metrics

We have selected 7 evaluation metrics to assess usability, privacy, and deployability. For usability assessment, we employ **Test Accuracy (Test ACC)**, which evaluates the final performance of the

model protected by defense techniques on the test dataset. Regarding privacy assessment, we initially utilize **MSE**, **Peak Signal-to-Noise Ratio (PSNR)**, and **Structural Similarity Index (SSIM)** to evaluate the effectiveness of MIA on reconstructing the input data of the protected model [52]. Here, a higher MSE and lower PSNR and SSIM (ranging from 0 to 1) indicate better defense effectiveness. Compared to the former two, SSIM focuses more on the perceptual quality of the image, encompassing luminance, contrast, and structural information. In addition to these, we also employ MINE [4], as mentioned in Section 4.3, to assess **Mutual Information (MI)** (ranging from 0 to 1) and the **Effective Information Mean**  $\delta(z)$ , which is the mean of the non-zero information output by the edge model on the test dataset. The specific training methods and model architecture for MINE are referenced from xxx. For deployability, we consider the **Edge model’s parameter count**  $|\theta_{\text{edge}}|$  and Inference Latency. The model parameter count directly determines memory or GPU memory occupation, while inference latency is tested on both CPU and GPU.

## 6.3 Experimental Results

1) *The effect of various defenses on the MI and  $\delta(z)$ .* the effectiveness of defenses is reflected by MI and  $\delta(z)$ , aligning with the criterion  $D_{\text{mia}}$  and the theoretical analysis presented in Section 4. Specifically, unprotected edge models show significant vulnerability to input reconstruction under both types of MIAs, with MI at 0.0566, MSE below 0.01, and SSIM exceeding 0.98. When protected by Perturbation-based defenses, all methods except NLS exhibit over a 10% drop in Test ACC. Moreover, these methods achieve only an 11% reduction in MI at most, demonstrating clear weaknesses against both MIAs. NLS shows a slight increase in mutual information for shallow neural networks, leading to weaker resistance to both types of attacks. Under IB-based defenses, usability sees a slight decline, but all methods except MID provide strong resistance against MLE-based MIA, with MSE values exceeding 0.5. Among these techniques, only BiDO significantly impacts MI and  $\delta(z)$ , providing effective defense, but its parameter selection and kernel width configuration (as shown in the table) are challenging, limiting its generalizability—a limitation further evidenced in subsequent experiments. This experiment adheres to the InfoSCISSORS setup, providing CLUB with a complete dataset and sufficient training iterations to ensure convergence. While CLUB effectively defends against MLE-based MIA, it struggles under the experimental conditions to resist Gen-based MIA and results in a 4.83% accuracy loss. Under AE-based defenses, target model usability improves, likely because the original model lacked sufficient capacity for optimal task classification, and the added model complexity enhanced performance. Additionally, MI indicates notable reductions in mutual information, showcasing reasonable defense effectiveness. However, in gray-box scenarios, AE-based defenses show reduced resistance, and the added complexity imposes a eightfold storage burden on edge models, as revealed by  $|\theta_{\text{edge}}|$ . SiftFunnel achieves the best defense performance against both MIAs while maintaining an accuracy loss below 3%. For MLE-based MIA, it achieves an MSE of 0.6792, and for Gen-based MIA, an MSE above 0.1. In gray-box scenarios, it maintains an MSE of 0.06 and an SSIM of 0.7647, ensuring robust resistance. Furthermore, MI and  $\delta(z)$

**Table 2: Quantitative evaluation of CNN on CIFAR-10 with different defenses against two MIAs.  $\uparrow$  indicates higher is better,  $\downarrow$  indicates lower is better. Bolded values are the best. Blue highlights show unprotected baseline performance, red indicates increased edge device load, yellow indicates reduced load, and gray shows gray-box defense performance.**

Method Class	Method	Test ACC $\uparrow$	MLE-based Attack [18]			Gen-based Attack [20]			MI $\downarrow$	$\delta(z)\downarrow$	$ \theta_{edge}\downarrow$
			MSE $\uparrow$	PSNR $\downarrow$	SSIM $\downarrow$	MSE $\uparrow$	PSNR $\downarrow$	SSIM $\downarrow$			
Unprotected		88.28%	0.0045	28.3421	0.9883	0.0017	32.5498	0.9987	0.0566	32,549	299,520
Perturbation-based	Adding noise [20] ( $\sigma = 0.8$ )	74.85% (-13.43%)	0.0291	20.1511	0.9135	0.0172	22.4249	0.9299	0.0502	65,535	299,520
	Dropping [20] ( $r = 0.8$ )	21.18% (-67.10%)	0.0127	23.7340	0.9609	0.0135	23.4835	0.9481	0.0501	6,509	
	DPSGD [1] (20, $1e-5$ )	61.83% (-26.45%)	0.0218	21.3868	0.9479	0.0016	32.4800	0.994	0.0623	39,829	
	NLS [43] ( $\alpha = -0.05$ )	87.60% (-0.68%)	0.0002	42.2684	0.9996	0.0014	33.3732	0.9949	0.0573	47,183	
IB-based	MID [45] ( $1e-2$ )	81.53% (-6.75%)	1.74e-5	50.4675	0.9999	0.0013	34.5184	0.9967	0.0584	45,198	299,520
	BiDO [34] (2; 20)	84.12% (-4.16%)	0.6699	6.5111	0.0138	0.035	19.2965	0.8751	0.0429	3,345	
	VIB [47]	88.21% (-0.07%)	0.5552	7.3264	0.0358	0.0042	28.5054	0.9842	0.0551	18,069	
	InfoScissors [10]	83.46% (-4.83%)	0.5715	7.2007	0.1345	0.0062	26.8799	0.9948	0.0549	43,364	
NND & IB-based	AE-based [3]	<b>90.56% (+2.28%)</b>	0.6345	6.7472	0.0051	0.0542	17.4852	0.8151	0.0358	2,617	2,365,056
	<b>SiftFunnel</b>	85.49% (-2.79%)	<b>0.6792</b>	<b>6.4510</b>	<b>0.0051</b>	<b>0.1166</b>	<b>14.1112</b>	<b>0.5419</b>	<b>0.0167</b>	<b>1,006</b>	<b>14,911</b>

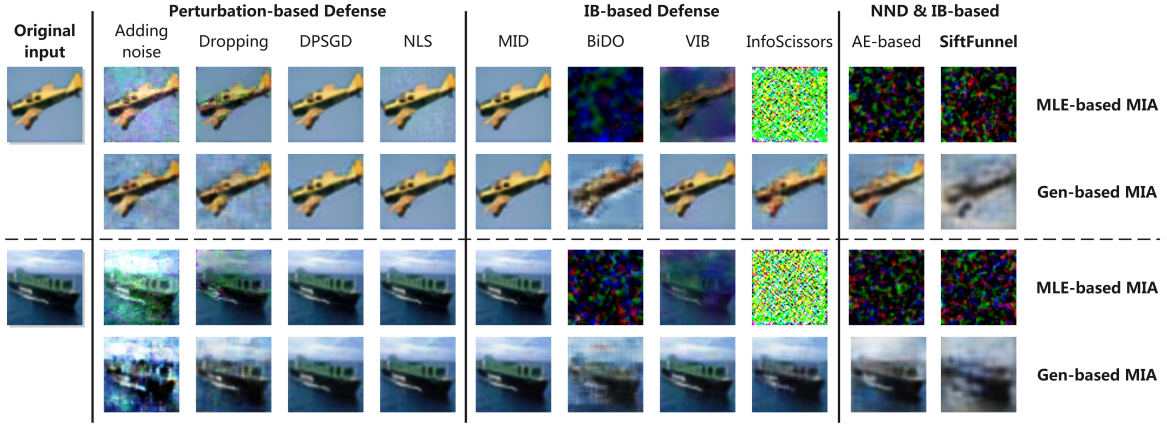


**Figure 4: A visual evaluation of the attack effectiveness of two MIAs on CNN edge models protected by various defense techniques, with NND & IB-based results specifically reflecting the gray-box scenario.**

**Table 3: Quantitative evaluation of the resistance to MIA across different architectures on CIFAR-10. The edge model divisions for CNN and ResNet-18 follow the configurations in Tables 2 and 4, while for VGG16, the edge model is set at the first ReLU layer after a max-pooling operation.**

Architecture	Test ACC $\uparrow$	MLE-based Attack [19]			Gen-based Attack [20]			MI $\downarrow$	$\delta(z)\downarrow$	$ \theta_{edge}\downarrow$
		MSE $\uparrow$	PSNR $\downarrow$	SSIM $\downarrow$	MSE $\uparrow$	PSNR $\downarrow$	SSIM $\downarrow$			
CNN	85.49% (-2.79%)	0.6792	6.4510	0.0051	0.1166	14.1112	0.5419	0.0167	1,006	14,911
ResNet-18	88.43% (-2.00%)	0.6538	6.6166	0.0059	0.1957	11.8562	0.0793	0.4772	4,028	78,864
VGG16	88.89% (-2.18%)	0.7801	5.8450	0.0005	0.2790	10.3230	0.3001	0.0128	3,587	52,086

demonstrate that SiftFunnel exerts optimal influence on the key elements of  $D_{mia}$ . Additionally,  $|\theta_{edge}|$  reveals that SiftFunnel reduces the edge model’s load by nearly 20 times.

2) *The effect of model architecture.* Changing the model architecture does not affect the parameter settings of the proposed method, which remain consistent with Section 6.1. We adapt the model to a ResNet-18 with skip connections, using the first residual block as the edge model. This setup is challenging for defense techniques, as shallow networks are simple and do not alter spatial dimensions. Table 4 shows minimal MI impact in unprotected models, leading to weak resistance against MIAs, with MLE-based MIA achieving an MSE of  $10^{-4}$  and Gen-based MIA  $10^{-3}$ . Under these conditions, existing perturbation-based defenses fail to balance usability and privacy effectively, resulting in poor defense performance. Among IB-based defenses, only VIB demonstrates resistance to MLE-based MIA by leveraging the estimation of  $I(x, z)$  as a loss to optimize the edge model. However, its effectiveness remains limited, particularly against Gen-based MIA. For BiDO, despite following the kernel bandwidth estimation methods from [34] and performing extensive experimental tuning, it fails to provide a configuration that

**Table 4: Quantitative evaluation of ResNet-18 on CIFAR-10 with different defenses against two MIAs. The target edge model is the first residual block of ResNet-18.  $\uparrow$  indicates higher is better,  $\downarrow$  indicates lower is better. Bolded values are the best. The meanings of color-coded regions are consistent with those in Table 2.**

Method Class	Method	Test ACC $\uparrow$	MLE-based Attack [18]			Gen-based Attack [20]			MI $\downarrow$	$\delta(z)\downarrow$	$ \theta_{\text{edge}} \downarrow$
			MSE $\uparrow$	PSNR $\downarrow$	SSIM $\downarrow$	MSE $\uparrow$	PSNR $\downarrow$	SSIM $\downarrow$			
Unprotected		90.43%	0.0001	71.0996	0.9991	0.0010	34.6599	0.9991	0.9719	182,134	149,824
Perturbation-based	Adding noise [20] ( $\sigma = 2$ )	81.39% (-9.04%)	0.0035	29.3354	0.9872	0.0054	27.4167	0.9794	0.9619	262,144	149,824
	Dropping [20] ( $r = 0.8$ )	14.09% (-76.34%)	0.0069	26.3641	0.9754	0.0077	25.9334	0.9711	0.9514	35,574	
	DPSGD [1] (20, $1e-5$ )	61.85% (-28.58%)	0.1901	11.9821	0.7172	0.0060	26.9751	0.9802	0.9515	178,956	
	NLS [43] ( $\alpha = -0.05$ )	88.57% (-1.86%)	0.0034	29.5001	0.9894	0.0011	34.4231	0.9961	0.9718	176,456	
IB-based	MID [45] ( $1e-2$ )	79.48% (-10.95%)	1.42e-7	73.2595	0.9999	0.0010	34.5893	0.9965	0.9729	173,587	149,824
	BiDO [34] (5; 10)	<b>90.08%</b> (-0.35%)	4.38e-7	68.3603	0.9999	0.0020	31.7621	0.9927	0.9647	219,832	
	VIB [47]	89.18% (-1.25%)	0.5869	7.0853	0.0216	0.0020	31.7621	0.9928	0.9402	54,800	
	InfoSCISSORS [10]	88.03% (-2.40%)	3.10e-5	49.8548	0.9999	0.0058	27.1608	0.9799	0.8927	216,919	
NND & IB-based	AE-based [3]	89.19% (-1.24%)	0.6543	6.6189	0.1243	0.0143	23.2332	0.9488	0.9397	74,356	279,136
	<b>SiftFunnel</b>	88.43% (-2.00%)	<b>0.6538</b>	<b>6.6166</b>	<b>0.0059</b>	<b>0.1957</b>	<b>11.8562</b>	<b>0.0793</b>	<b>0.4772</b>	<b>4,028</b>	<b>78,864</b>

**Table 5: Quantitative evaluation of different defense methods in protecting CNN against MIAs on the FaceScrub dataset. Changes in data types alter the inference task, requiring adjustments to the parameters of the defense methods.**

Method Class	Method	Test ACC $\uparrow$	MLE-based Attack [19]			Gen-based Attack [20]			MI $\downarrow$	$\delta(z)\downarrow$	$ \theta_{\text{edge}} \downarrow$
			MSE $\uparrow$	PSNR $\downarrow$	SSIM $\downarrow$	MSE $\uparrow$	PSNR $\downarrow$	SSIM $\downarrow$			
Unprotected		88.31%	0.0005	37.6115	0.9972	0.0006	32.4108	0.9908	0.0514	45,271	299,520
Perturbation-based	NLS [43] ( $\alpha = -0.2$ )	87.97% (-0.34%)	0.0004	38.8904	0.9980	0.0018	32.3274	0.9906	0.0496	44,783	299,520
IB-based	MID [45] ( $1e-2$ )	79.45% (-10.98%)	0.0017	32.3435	0.9897	0.0018	32.1285	0.9901	0.0507	39,277	299,520
	BiDO [34] (2; 20)	88.02% (-0.29%)	0.0004	39.0838	0.9978	0.0018	32.2048	0.9904	0.0493	44,915	
	VIB [47]	<b>88.05%</b> (-0.26%)	0.7354	6.1060	0.0032	0.0033	29.5697	0.9823	0.0493	15,649	
	InfoSCISSORS [10]	81.61% (-6.70%)	<b>0.7449</b>	<b>6.0504</b>	<b>0.0026</b>	0.0060	26.9803	0.9675	0.0408	57,050	
NND & IB-based	AE-based [3]	83.45 (-4.86%)	0.6474	6.6594	0.0090	<b>0.0609</b>	<b>16.9260</b>	<b>0.6656</b>	0.0238	<b>585</b>	2,365,056
	<b>SiftFunnel</b> ( $\lambda_1 = 5.0, \lambda_2 = 0.1, \lambda_3 = 0.1$ )	85.39% (-2.92%)	0.7264	6.1593	0.0060	0.0559	17.3018	0.6854	<b>0.0104</b>	637	<b>14,911</b>

balances usability and privacy, ultimately leading to suboptimal defense outcomes. InfoSCISSORS demonstrates some impact on MI under this configuration, but the increase in  $\delta(z)$  undermines its defense effectiveness against Gen-based MIA, showing only marginal improvements. AE-based defenses exhibit certain resistance to attacks on low-dimensional features in earlier stages, but under the ResNet configuration, their performance diminishes. While this method reduces  $\delta(z)$  by 60%, it has minimal impact on MI, with only a 0.04% decrease. Consequently, AE-based defenses struggle to counter both black-box and gray-box Gen-based MIAs effectively.

In contrast, SiftFunnel reduces MI by 50% and lowers  $\delta(z)$  to the millesimal scale, achieving the best resistance against MIAs while maintaining usability and deployability. Notably, it achieves a minimum SSIM of 0.0793, highlighting its superior performance in balancing privacy and usability.

3) *The effect of data type.* Changes in data types lead to shifts in task requirements. For instance, in this study, the facial recognition task involves 530 classes, while ChestX-ray classification involves 4 classes, necessitating parameter adjustments as shown in Table 5. As

analyzed in the previous section on model architectures, to achieve better defense performance, we adjusted the edge model divisions for ResNet-18 and VGG. Specifically, the division points were set after the second residual block for ResNet and after the first ReLU layer following the second max-pooling layer for VGG. The results, summarized in the table 5, show that the defense performance remains unaffected by changes in data types. SiftFunnel continues to be the best defense method, offering an optimal balance between usability, privacy, and deployability.

4) *Ablation Study.* To validate the effectiveness of SiftFunnel’s model structure and loss function design, as well as its defense capability, we conducted ablation experiments using Gen-based MIA. As shown in Table 6, we separately removed the Information Funnel and Attention Blocks from the model structure. The results indicate that removing the Funnel had minimal impact on accuracy, with only a 0.1% decrease, while removing the attention mechanism led to a significant increase in MI compared to SiftFunnel. For the loss function, we evaluated the impact of individually removing KL divergence, linear and nonlinear constraints, and the  $l_1$ -norm. The

**Table 6: SiftFunnel Ablation Study on CIFAR-10. The target edge model is the first residual block of ResNet-18, with Gen-based MIA as the attack method. The Red area indicates the strong attack hypothesis from Section 5.2.**

Method	Test ACC↑	MSE↑	PSNR↓	SSIM↓	MI↓	$\delta(z)$ ↓
Unprotected	90.43%	0.0010	34.6599	0.9991	0.9719	182,134
Without Funnel (Average training round takes 1 minute, batchsize=64)	<b>90.33% (-0.10%)</b>	0.0594	17.0709	0.7776	0.8945	24,322
Without Attention Blocks	88.45% (-1.98%)	0.0525	17.5709	0.8178	0.8763	<b>3,904</b>
Without KL and LS	88.59% (-1.84%)	0.0850	15.4813	0.6905	0.7935	3,994
Without $\mathcal{L}_{dCor}$	88.77% (-1.66%)	0.0268	20.4929	0.9025	0.9505	4,013
Without $\mathcal{L}_{Pearson}$	88.83% (-1.60%)	0.0492	17.8576	0.8294	0.8618	4,037
Without $l_1$	88.48% (-1.95%)	0.0789	15.8057	0.7272	0.8158	4,030
Attack SiftFunnel in Cloud	88.43% (-2.00%)	0.0521	17.6159	0.8205	0.8905	176,380
SiftFunnel		<b>0.2790</b>	<b>10.3230</b>	<b>0.3001</b>	<b>0.4772</b>	4,028

results demonstrate that KL divergence and  $l_1$ -norm moderately improved defense, whereas nonlinear constraints played a critical role; removing them increased the MSE to 0.0268. Additionally, we verified the hypothesis from Section 5.2, showing that even when adversaries reconstructed input using features from the cloud’s compensation module, SiftFunnel outperformed existing defenses in protecting transmitted features.

We also evaluated the processing speed of the edge model on both CPU and GPU under this configuration. For single-sample input, the unprotected edge model had a CPU latency of 1.204ms, the AE-based protected model had 2.812ms, and SiftFunnel achieved 2.192ms. On GPU, the processing latency was 3.9ms, 4.3ms, and 6.9ms, respectively. While SiftFunnel showed slightly higher latency on GPU, it required significantly less memory, enabling more parallel processing of inputs under the same resource constraints.

## 7 DISCUSSION

Systematic experiments validated both the criterion and the effectiveness of the method. However, our analysis revealed that achieving optimal resistance against attacks remains challenging for current defense methods, including SiftFunnel, particularly when applied to shallow edge neural networks. When edge models perform only basic feature processing, even SiftFunnel can still allow Gen-based MIA to reconstruct blurred feature structures, while other methods are more vulnerable to input reconstruction. Enhancing privacy protection for extremely shallow edge neural networks presents a promising direction for future research.

Additionally, using MI as an evaluation metric, we observed that some defense methods result in only a 0.5% reduction in MI between inputs and features, yet current MLE-based MIAs still fail to bypass these defenses. This is directly linked to the lack of advancement in existing attack methods. Based on our experimental findings, we suggest that further exploration of more powerful MIAs in white-box scenarios could be a potential research direction.

## 8 CONCLUSION

The increasing complexity of neural networks and inference tasks, alongside the demand for efficiency and real-time feedback, presents

significant challenges for edge devices with limited resources. Collaborative inference offers a solution by delegating feature extraction to edge devices and offloading subsequent tasks to the cloud, but this process leaves transmitted features vulnerable to MIAs. To address these vulnerabilities, we established a first criterion  $D_{mia}$  for evaluating MIA difficulty and proposed SiftFunnel, a privacy-preserving framework designed to limit redundant information and enhance usability. By integrating linear and non-linear correlation constraints, label smoothing, and a funnel-shaped edge model with attention mechanisms, SiftFunnel achieves robust privacy protection while maintaining usability and deployability. Experimental results demonstrate its effectiveness, achieving superior defense against MIAs with minimal accuracy loss and a balanced trade-off among usability, privacy, and practicality.

## REFERENCES

- [1] Martin Abadi, Andy Chu, Ian Goodfellow, H Brendan McMahan, Ilya Mironov, Kunal Talwar, and Li Zhang. 2016. Deep learning with differential privacy. In *Proceedings of the 2016 ACM SIGSAC conference on computer and communications security*. 308–318.
- [2] Kenneth J Arrow. 1969. Classificatory notes on the production and transmission of technological knowledge. *The American Economic Review* 59, 2 (1969), 29–35.
- [3] Bardia Azizian and Ivan V Bajić. 2024. Privacy-Preserving Autoencoder for Collaborative Object Detection. *IEEE Transactions on Image Processing* (2024).
- [4] Mohamed Ishmael Belghazi, Aristide Baratin, Sai Rajeshwar, Sherjil Ozair, Yoshua Bengio, Aaron Courville, and Devon Hjelm. 2018. Mutual information neural estimation. In *International conference on machine learning*. PMLR, 531–540.
- [5] Pengyu Cheng, Weituo Hao, Shuyang Dai, Jiachang Liu, Zhe Gan, and Lawrence Carin. 2020. Club: A contrastive log-ratio upper bound of mutual information. In *International conference on machine learning*. PMLR, 1779–1788.
- [6] Israel Cohen, Yiteng Huang, Jingdong Chen, Jacob Benesty, Jacob Benesty, Jingdong Chen, Yiteng Huang, and Israel Cohen. 2009. Pearson correlation coefficient. *Noise reduction in speech processing* (2009), 1–4.
- [7] Sayanton V Dibbo. 2023. Sok: Model inversion attack landscape: Taxonomy, challenges, and future roadmap. In *2023 IEEE 36th Computer Security Foundations Symposium (CSF)*. IEEE, 439–456.
- [8] Shiwei Ding, Lan Zhang, Miao Pan, and Xiaoyong Yuan. 2024. PATROL: Privacy-Oriented Pruning for Collaborative Inference Against Model Inversion Attacks. In *Proceedings of the IEEE/CVF Winter Conference on Applications of Computer Vision*. 4716–4725.
- [9] Monroe D Donsker and SR Srinivasa Varadhan. 1983. Asymptotic evaluation of certain Markov process expectations for large time. IV. *Communications on pure and applied mathematics* 36, 2 (1983), 183–212.
- [10] Lin Duan, Jingwei Sun, Yiran Chen, and Maria Gorlatova. 2023. PrivaScissors: Enhance the Privacy of Collaborative Inference through the Lens of Mutual Information. *arXiv preprint arXiv:2306.07973* (2023).

- [11] Apple Security Engineering and Architecture. 2024. *Private Cloud Compute: A new frontier for AI privacy in the cloud*.
- [12] Matt Fredrikson, Somesh Jha, and Thomas Ristenpart. 2015. Model inversion attacks that exploit confidence information and basic countermeasures. In *Proceedings of the 22nd ACM SIGSAC conference on computer and communications security*. 1322–1333.
- [13] Matthew Fredrikson, Eric Lantz, Somesh Jha, Simon Lin, David Page, and Thomas Ristenpart. 2014. Privacy in pharmacogenetics: An {End-to-End} case study of personalized warfarin dosing. In *23rd USENIX security symposium (USENIX Security 14)*. 17–32.
- [14] Lovedeep Gondara. 2016. Medical image denoising using convolutional denoising autoencoders. In *2016 IEEE 16th international conference on data mining workshops (ICDMW)*. IEEE, 241–246.
- [15] Arthur Gretton, Olivier Bousquet, Alex Smola, and Bernhard Schölkopf. 2005. Measuring statistical dependence with Hilbert-Schmidt norms. In *International conference on algorithmic learning theory*. Springer, 63–77.
- [16] Arthur Gretton, Ralf Herbrich, Alexander Smola, Olivier Bousquet, Bernhard Schölkopf, and Aapo Hyvärinen. 2005. Kernel methods for measuring independence. *Journal of Machine Learning Research* 6, 12 (2005).
- [17] Koh Jun Hao, Sy-Tuyen Ho, Ngoc-Bao Nguyen, and Ngai-Man Cheung. 2025. On the Vulnerability of Skip Connections to Model Inversion Attacks. In *European Conference on Computer Vision*. Springer, 140–157.
- [18] Kaiming He, Xiangyu Zhang, Shaoqing Ren, and Jian Sun. 2016. Deep residual learning for image recognition. In *Proceedings of the IEEE conference on computer vision and pattern recognition*. 770–778.
- [19] Zecheng He, Tianwei Zhang, and Ruby B Lee. 2019. Model inversion attacks against collaborative inference. In *Proceedings of the 35th Annual Computer Security Applications Conference*. 148–162.
- [20] Zecheng He, Tianwei Zhang, and Ruby B Lee. 2020. Attacking and protecting data privacy in edge-cloud collaborative inference systems. *IEEE Internet of Things Journal* 8, 12 (2020), 9706–9716.
- [21] Sy-Tuyen Ho, Koh Jun Hao, Keshigeyan Chandrasegaran, Ngoc-Bao Nguyen, and Ngai-Man Cheung. 2024. Model Inversion Robustness: Can Transfer Learning Help?. In *Proceedings of the IEEE/CVF Conference on Computer Vision and Pattern Recognition*. 12183–12193.
- [22] Fanliang Hu, Jian Shen, and Pandi Vijayakumar. 2023. Side-Channel Attacks Based on Multi-Loss Regularized Denoising AutoEncoder. *IEEE Transactions on Information Forensics and Security* (2023).
- [23] Jie Hu, Li Shen, and Gang Sun. 2018. Squeeze-and-excitation networks. In *Proceedings of the IEEE conference on computer vision and pattern recognition*. 7132–7141.
- [24] Jacob Huckelberry, Yuke Zhang, Allison Sansone, James Mickens, Peter A Beerel, and Vijay Janapa Reddi. 2024. TinyML Security: Exploring Vulnerabilities in Resource-Constrained Machine Learning Systems. *arXiv preprint arXiv:2411.07114* (2024).
- [25] Shuaifan Jin, He Wang, Zhibo Wang, Feng Xiao, Jiahui Hu, Yuan He, Wenwen Zhang, Zhongjie Ba, Weijie Fang, Shuhong Yuan, et al. 2024. {FaceObfuscator}: Defending Deep Learning-based Privacy Attacks with Gradient Descent-resistant Features in Face Recognition. In *33rd USENIX Security Symposium (USENIX Security 24)*. 6849–6866.
- [26] Alex Krizhevsky, Geoffrey Hinton, et al. 2009. Learning multiple layers of features from tiny images. (2009).
- [27] Runze Li, Wei Zhong, and Liping Zhu. 2012. Feature screening via distance correlation learning. *J. Amer. Statist. Assoc.* 107, 499 (2012), 1129–1139.
- [28] Rongke Liu, Dong Wang, Yizhi Ren, Zhen Wang, Kaitian Guo, Qianqian Qin, and Xiaolei Liu. 2024. Unstoppable Attack: Label-Only Model Inversion via Conditional Diffusion Model. *IEEE Transactions on Information Forensics and Security* (2024).
- [29] Ziwei Liu, Ping Luo, Xiaogang Wang, and Xiaoou Tang. 2015. Deep learning face attributes in the wild. In *Proceedings of the IEEE international conference on computer vision*. 3730–3738.
- [30] Shagufta Mehnaz, Sayanton V Dibbo, Roberta De Viti, Ehsanul Kabir, Björn B Brandenburg, Stefan Mangard, Ninghui Li, Elisa Bertino, Michael Backes, Emiliano De Cristofaro, et al. 2022. Are your sensitive attributes private? novel model inversion attribute inference attacks on classification models. In *31st USENIX Security Symposium (USENIX Security 22)*. 4579–4596.
- [31] Fatemehsadat Mireshghallah, Mohammadkazem Taram, Ali Jalali, Ahmed Taha Taha Elthakeb, Dean Tullsen, and Hadi Esmaeilzadeh. 2021. Not all features are equal: Discovering essential features for preserving prediction privacy. In *Proceedings of the Web Conference 2021*. 669–680.
- [32] Diganta Misra, Triyak Nalamada, Ajay Uppili Arasanipalai, and Qibin Hou. 2021. Rotate to Attend: Convolutional Triplet Attention Module. In *2021 IEEE Winter Conference on Applications of Computer Vision (WACV)*. 3138–3147. <https://doi.org/10.1109/WACV48630.2021.00318>
- [33] Hong-Wei Ng and Stefan Winkler. 2014. A data-driven approach to cleaning large face datasets. In *2014 IEEE international conference on image processing (ICIP)*. IEEE, 343–347.
- [34] Xiong Peng, Feng Liu, Jingfeng Zhang, Long Lan, Junjie Ye, Tongliang Liu, and Bo Han. 2022. Bilateral dependency optimization: Defending against model-inversion attacks. In *Proceedings of the 28th ACM SIGKDD Conference on Knowledge Discovery and Data Mining*. 1358–1367.
- [35] Yuben Qu, Hao Sun, Chao Dong, Jiawen Kang, Haipeng Dai, Qihui Wu, and Song Guo. 2023. Elastic collaborative edge intelligence for UAV swarm: Architecture, challenges, and opportunities. *IEEE Communications Magazine* (2023).
- [36] Jorma J Rissanen. 1996. Fisher information and stochastic complexity. *IEEE transactions on information theory* 42, 1 (1996), 40–47.
- [37] Leonid I Rudin, Stanley Osher, and Emad Fatemi. 1992. Nonlinear total variation based noise removal algorithms. *Physica D: nonlinear phenomena* 60, 1-4 (1992), 259–268.
- [38] Unais Sait, K Lal, S Prajapati, Rahul Bhaumik, Tarun Kumar, S Sanjana, and Kriti Bhalla. 2020. Curated dataset for covid-19 posterior-anterior chest radiography images (x-rays). *Mendeley Data* 1, J (2020).
- [39] Nir Shlezinger and Ivan V Bajić. 2022. Collaborative inference for AI-empowered IoT devices. *IEEE Internet of Things Magazine* 5, 4 (2022), 92–98.
- [40] Nir Shlezinger, Erez Farhan, Hai Morgenstern, and Yonina C Eldar. 2021. Collaborative inference via ensembles on the edge. In *ICASSP 2021-2021 IEEE International Conference on Acoustics, Speech and Signal Processing (ICASSP)*. IEEE, 8478–8482.
- [41] Karen Simonyan. 2014. Very deep convolutional networks for large-scale image recognition. *arXiv preprint arXiv:1409.1556* (2014).
- [42] Lukas Struppek, Dominik Hintersdorf, Antonio De Almeida Correia, Antonia Adler, and Kristian Kersting. 2022. Plug & play attacks: Towards robust and flexible model inversion attacks. *arXiv preprint arXiv:2201.12179* (2022).
- [43] Lukas Struppek, Dominik Hintersdorf, and Kristian Kersting. 2023. Be careful what you smooth for: Label smoothing can be a privacy shield but also a catalyst for model inversion attacks. *arXiv preprint arXiv:2310.06549* (2023).
- [44] Christian Szegedy, Sergey Ioffe, Vincent Vanhoucke, and Alexander Alemi. 2017. Inception-v4, inception-resnet and the impact of residual connections on learning. In *Proceedings of the AAAI conference on artificial intelligence*, Vol. 31.
- [45] Tianhao Wang, Yuheng Zhang, and Ruoxi Jia. 2021. Improving robustness to model inversion attacks via mutual information regularization. In *Proceedings of the AAAI Conference on Artificial Intelligence*, Vol. 35. 11666–11673.
- [46] Yulong Wang, Xingshu Chen, and Qixu Wang. 2022. Privacy-preserving Security Inference Towards Cloud-Edge Collaborative Using Differential Privacy. *arXiv preprint arXiv:2212.06428* (2022).
- [47] Yanhu Wang, Shuaishuai Guo, Yiqin Deng, Haixia Zhang, and Yuguang Fang. 2024. Privacy-preserving task-oriented semantic communications against model inversion attacks. *IEEE Transactions on Wireless Communications* (2024).
- [48] Sanghyun Woo, Jongchan Park, Joon-Young Lee, and In So Kweon. 2018. Cbam: Convolutional block attention module. In *Proceedings of the European conference on computer vision (ECCV)*. 3–19.
- [49] Yixiao Xu, Binxing Fang, Mohan Li, Xiaolei Liu, and Zhihong Tian. 2024. Query-Efficient Model Inversion Attacks: An Information Flow View. *IEEE Transactions on Information Forensics and Security* (2024).
- [50] Mengda Yang, Ziang Li, Juan Wang, Hongxin Hu, Ao Ren, Xiaoyang Xu, and Wenzhe Yi. 2022. Measuring data reconstruction defenses in collaborative inference systems. *Advances in Neural Information Processing Systems* 35 (2022), 12855–12867.
- [51] Ziqi Yang, Jiyi Zhang, Ee-Chien Chang, and Zhenkai Liang. 2019. Neural network inversion in adversarial setting via background knowledge alignment. In *Proceedings of the 2019 ACM SIGSAC Conference on Computer and Communications Security*. 225–240.
- [52] Yupeng Yin, Xianglong Zhang, Huanle Zhang, Feng Li, Yue Yu, Xiuzhen Cheng, and Pengfei Hu. 2023. Ginver: Generative model inversion attacks against collaborative inference. In *Proceedings of the ACM Web Conference 2023*. 2122–2131.
- [53] Xiaojian Yuan, Kejiang Chen, Jie Zhang, Weiming Zhang, Nenghai Yu, and Yang Zhang. 2023. Pseudo label-guided model inversion attack via conditional generative adversarial network. In *Proceedings of the AAAI Conference on Artificial Intelligence*, Vol. 37. 3349–3357.
- [54] Huan Zhang, Hongge Chen, Zhao Song, Duane Boning, Inderjit S Dhillon, and Cho-Jui Hsieh. 2019. The limitations of adversarial training and the blind-spot attack. *arXiv preprint arXiv:1901.04684* (2019).
- [55] Ruisi Zhang, Seira Hidano, and Farinaz Koushanfar. 2022. Text revealer: Private text reconstruction via model inversion attacks against transformers. *arXiv preprint arXiv:2209.10505* (2022).
- [56] Yuheng Zhang, Ruoxi Jia, Hengzhi Pei, Wenxiao Wang, Bo Li, and Dawn Song. 2020. The secret revealer: Generative model-inversion attacks against deep neural networks. In *Proceedings of the IEEE/CVF conference on computer vision and pattern recognition*. 253–261.
- [57] Zeping Zhang, Xiaowen Wang, Jie Huang, and Shuaishuai Zhang. 2023. Analysis and Utilization of Hidden Information in Model Inversion Attacks. *IEEE Transactions on Information Forensics and Security* (2023).
- [58] Xiaochen Zhu, Xinjian Luo, Yuncheng Wu, Yangfan Jiang, Xiaokui Xiao, and Beng Chin Ooi. 2023. Passive Inference Attacks on Split Learning via Adversarial Regularization. *arXiv preprint arXiv:2310.10483* (2023).